Theory of the response of an fcc crystal to [110] uniaxial loading

Frederick Milstein
*University of California, Santa Barbara, California 93106**
and Weizmann Institute of Science, Rehovot, Israel

K. Huang
University of California, Santa Barbara, California 93106
(Received 29 November 1976)

The response of an fcc crystal to unconstrained [110] uniaxial loading has been studied theoretically. Numerical calculations were made of load, stress (σ_{110}), lattice parameters, and elastic moduli (C_{rs}) along the primary loading path, and the domain of M stability (as defined by Hill and Milstein) was determined. The crystal model was that used by Huang *et al.* to study the shear of a crystal. In tension, the limit of M stability was at the maximum load (with corresponding $\sigma_{110} = 8.78 \times 10^{10}$ dyn/cm^2 at a strain of 7.5%; these values are comparable to other estimates of the "theoretical strength" of crystals, including experimental values of whisker strengths). The domain of M stability in compression was remarkably large, and the magnitude of σ_{110} in compression at the limit of M stability was about 100 times the maximum tensile stress. With very large compression, the Poisson's ratios along the two principal axes normal to the load approached zero, and the lattice tended to arrange itself with successive planes in a particular "two-dimensional close-packed relationship." This latter tendency, in a sense, can "explain" the difference in algebraic sign of the Poisson's ratios along the principal axes normal to the [110] direction in some fcc crystals. In elongation, the primary equilibrium path intersects the path corresponding to unconstrained [100] uniaxial loading of a fcc or bcc crystal at the invariant eigenstate $C_{22} = C_{23}$. The Poisson's ratios approach infinity as this state is approached along a primary equilibrium (but unstable) path. Such studies of crystal response are of interest in a variety of applications, including, possibly, martensitic transformations.

I. INTRODUCTION

Previous papers have reported, in detail, the theoretical response of ideal simple crystals to [100] uniaxial loading[1,2] and to shear forces applied to the (100) plane in the [010] direction.[3] In the present paper we give a detailed account of the theoretical response of an fcc crystal to [110] uniaxial loading. In order to perform numerical calculations, a relatively simple model for interatomic interactions in the crystal has been employed. Nevertheless, the results have exhibited a variety of interesting behaviors (not all of which could have been anticipated beforehand) and thereby provide insights into the nature of possible phenomena during homogeneous, large strain deformation of crystals.

These studies are of particular interest in applications to systems in which large, elastic (but not necessarily linear) deformation may occur, i.e., in cases where large deformations may occur either without significant dislocation movement or before deformation by dislocation movement becomes dominant. Relevant examples may include (i) deformation of whiskers, (ii) martensitic transformations, (iii) very rapid shock deformation (e.g., if the rate of deformation is greater than the dislocation velocity), (iv) powder technology and size reduction (e.g., the "theoretical strength" of solids forms a basis for calculating the efficiency of grinding processes), and (v) mechanical properties of small structures such as metallized integrated circuit structures (presuming that regions relatively free of defects can occur).

II. CRYSTAL MODEL

The potential energy of interaction $\phi(r)$ between any two atoms in the crystal is assumed to consist of an attractive and a repulsive term, each of which depends exponentially upon interactive spacing r. In Ref. 4, explicit functions $\phi(r)$ were determined for a number of cubic crystals (from the stress-free lattice parameter and elastic constants C_{11} and C_{12}) and the applicability (and limitations) of such a model was discussed. Subsequent studies[2,3] of the response of a crystal to selected modes of loading employed the particular set of functions ϕ that were determined[4] for the element nickel for the reasons that (i) among the fcc metals which were examined, Ni comes closest to obeying the Cauchy condition $C_{12} = C_{44}$; (ii) reasonably good agreement was obtained between theoretical and experimental pressure-volume relations in the region of anharmonic behavior; (iii) the theoretical model exhibits a reasonably accurate stress-strain curve in the linear region (since experimental values of elastic moduli were used to determine the atomic parameters defining ϕ). Included in this set of functions ϕ were both short-range,

steep functions and long-range, shallow functions. For example, in the "steepest" potential ϕ employed in the calculations, about 92% of the cohesive energy per atom in the crystal comes from nearest-neighbor interactions and less than 0.1% from, say, all of the sixth- or seventh-near-neighbor interactions; whereas in the "shallowest" potential, only about 51% of this cohesive energy can be attributed to nearest-neighbor interactions, while as much as 3.1% comes from seventh-near neighbors. Nevertheless, the model was found to be self-consistent in the sense that the response of the crystal, even after very large strains, was found to be surprisingly insensitive to the details of the function ϕ (assuming, of course, that the same empirical data were used to specify each function ϕ in the set).

In view of these considerations, calculations in the present study are carried out using one of the functions ϕ employed in the previous studies.[2,3] We arbitrarily selected the particular function for which the repulsive exponent is twice the attractive exponent (often referred to as the Morse function), viz.

$$\phi(r) = D(e^{-2\alpha(r-r_0)} - 2e^{-\alpha(r-r_0)}), \tag{1}$$

with $D = 0.35059 \times 10^{-12}$ erg, $\alpha a^0 = 8.7660$, and $r_0/a^0 = 0.71727$; the value of the stress-free lattice parameter $a^0 = 3.5238$ Å.

Because of the simplicity of the crystal model, we are more interested in exploring the qualitative or semiquantitative behavior of the crystal than in presenting the specific numerical results. Nevertheless, since the numerical parameters describing the crystal model are derived from experiment, and since the quantitative results are not unreasonable, we also report our results quantitatively.

Figure 1 illustrates a portion of an initially fcc lattice that is subjected to [110] uniaxial stress. A face-centered (fc) unit cell (which is initially cubic) is shown with "solid centers"; four body-centered (bc) unit cells, each with edges b_1, b_2, and b_3, are also shown. The applied force is parallel to edge b_1 and perpendicular to edges b_2 and b_3. Thus edges b_1, b_2, and b_3 will remain mutually perpendicular throughout the loading path (at least for the stable crystal), and no shear forces act on the faces of the bc cell. The complete state of loading for the crystal is then specified [see Ref. 1, Eqs. (52)] by the three equations

$$F_i(b_1, b_2, b_3) = \tfrac{1}{2} b_i \sum_{l_1}\sum_{l_2}\sum_{l_3} l_i^2 \frac{\partial \phi(r)}{\partial (r^2)}, \quad i = 1, 2, 3, \tag{2}$$

where the F_i are the forces, acting in directions parallel to the respective b_i, on the faces of the bc cell. The applied stress in the [110] direction of the fc cell is then

$$\sigma_{110} = F_1/b_2 b_3; \tag{3}$$

to insure that this is indeed a uniaxial stress, the lattice parameters b_1, b_2, and b_3 must be such that

$$\sum_{l_1}\sum_{l_2}\sum_{l_3} l_i^2 \frac{\partial \phi}{\partial (r^2)} = 0, \quad i = 2, 3. \tag{4}$$

The summations in (2) and (4) are over the indices l_1, l_2, l_3 that identify the lattice sites in the crystal; the values of the summations depend upon the b_i, since the distance between the (arbitrarily selected) origin site and another site at l_1, l_2, l_3 is

$$r = \tfrac{1}{2}(l_1^2 b_1^2 + l_2^2 b_2^2 + l_3^2 b_3^2)^{1/2}. \tag{5}$$

The l_i are integers that must be either all even or all odd for a given site in the bc lattice. The operator $\partial/\partial(r^2)$ is the same as $(1/2r)(\partial/\partial r)$, and explicit expressions for the first and second derivatives of ϕ with respect to r^2 can be found in Refs. 2 and 3. The summations are performed over a sufficient number of lattice sites to obtain convergence to the desired number of significant figures. Starting from the state of zero stress, the lattice parameter b_1 can be increased (or decreased) by a small amount. The parameters b_2 and b_3 are then "relaxed," using a generalized Newton-Raphson method of iteration, until the summations in Eqs. (4) are zero. Then, the set b_1, b_2, b_3 is used in evaluating F_1 and σ_{110} from Eqs. (2) and (3), and the complete procedure is repeated. A positive stress indicates tension, and a negative is compression.

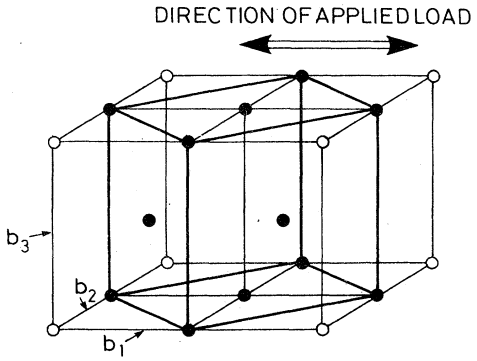

FIG. 1. Portion of the initially face-centered-cubic lattice, showing a face-centered unit cell (lattice sites shown with "solid centers") and four body-centered unit cells, each with edges b_1, b_2, b_3. The [110] stress (with respect to the fc cell) is parallel to edge b_1. (For clarity, the sites on the two "rear faces" of the fc cell are not indicated.)

III. IDEAL CRYSTAL STRENGTH

The concept of "ideal crystal strength," regarded as an instability of a loaded crystal, has been discussed in detail in a recent paper by Hill and Milstein.[5] Briefly, elastic moduli C_{rs} can be defined by

$$C_{rs} = \frac{\partial^2 W}{\partial q_r \partial q_s}, \qquad r,s = 1,\ldots,6, \tag{6}$$

where the q_r are geometrical variables or "coordinates" used to define the state of strain of the crystal, and W is the internal energy of the unit cell. These moduli, if known numerically along the prescribed loading path, can be used to examine the convexity of the internal energy W according to the positive definiteness of the quadratic form $C_{rs}\delta q_r \delta q_s$ (summation implied over repeated indices). In previous studies by a variety of authors,[1-3,6,7] the range over which the internal energy remains convex has been associated with the range of stability of the crystal, with the point of instability representing the "theoretical or ideal strength" of the crystal. However. as was first noted by Hill,[8] in a crystal under load, convexity of the internal energy is not coordinate invariant.

The three sets of geometrical variables principally favored in the literature are (i) the so-called Milstein or M variables (for $r = 1, 2, 3$, the q_r are the edges of the unit cell; and for $r = 4,5,6$, the q_r are the included angles), (ii) the components of the Green's tensor, and (iii) the components of the stretch tensor. Hill and Milstein[5] have employed the terms M strength, G strength, and S strength to indicate the ranges of deformation over which the respective Hessians $C_{rs}\delta q_r \delta q_s$ remain positive definite.

In the present study we calculate the Milstein moduli relative to the bc cell, along the primary path, using the relations[1]

$$C_{ij} = \tfrac{1}{4} b_i b_j \sum_{l_1}\sum_{l_2}\sum_{l_3} l_i^2 l_j^2 \frac{\partial^2 \phi(r)}{[\partial(r^2)]^2} + \tfrac{1}{2}\delta_{ij} \sum_{l_1}\sum_{l_2}\sum_{l_3} l_i^2 \frac{\partial \phi(r)}{\partial(r^2)}, \tag{7}$$

for $i,j \leq 3$, where δ_{ij} is the Kronecker delta. The bc cell is orthorhombic; thus, in general there are nine independent elastic constants. However, for the pairwise central force model there is a Cauchy-like symmetry among the M moduli, viz.,

$$C_{44} = b_2 b_3 C_{23}, \quad C_{55} = b_1 b_3 C_{13}, \quad C_{66} = b_1 b_2 C_{12}. \tag{8}$$

Thus, for a given state of strain, the number of independent M moduli is reduced to six. The C_{ij}, calculated from (7), are used to determine the range of M stability according to the criteria[3]

$$D_1 = C_{11} > 0, \quad D_2 = \begin{vmatrix} C_{11} & C_{12} \\ C_{12} & C_{22} \end{vmatrix} > 0,$$
$$D_3 = \begin{vmatrix} C_{11} & C_{12} & C_{13} \\ C_{12} & C_{22} & C_{23} \\ C_{13} & C_{23} & C_{33} \end{vmatrix} > 0, \tag{9}$$
$$C_{12} > 0, \quad C_{23} > 0, \quad \text{and} \quad C_{13} > 0.$$

One question of particular interest is whether the predictions of "stability," via the respective convexity criteria, depend sensitively upon the particular choices of strain variables. Although we do not attempt to answer this question in the present paper, we have taken a step in that direction in the sense that other sets of moduli C_{rs}^*, defined in terms of other sets of variables q_r^*, can be calculated directly from the known values of the M moduli and the state of strain and loading of the crystal.[5] It is intended, in the immediate future, to make such calculations, and thereby examine quantitatively the question of the sensitivity of the stability predictions to choice of strain variables, along the present loading path, as well as along the paths of Refs. 2 and 3 (for which the M moduli also have been calculated).

IV. RESULTS AND DISCUSSION

Figures 2 and 3 show the "initial" behavior of the crystal in compression and tension. (In order to facilitate comparison among the various figures presented herein, a number of states of the crystal are labeled in the figures with upper case letters; each letter indicates a particular state of strain and rotational orientation of the crystal.) It is convenient to think of the crystal as originally residing in the unloaded ($\sigma_{110} = F_1/b_2 b_3 = 0$) fcc state A, in which the fcc unit cell has the orientation, with respect to edges b_1, b_2, b_3, as shown in Fig. 1. In this state, the fcc lattice parameter $a^0 = 3.5238$ Å; the lattice parameters of the bc cell are, of course, $b_1^0 = b_2^0 = a^0/\sqrt{2} = 2.4917$ Å and $b_3^0 = a^0$; the energy $W = \sum_{l_1}\sum_{l_2}\sum_{l_3}\phi(r)$ is at a minimum. In the neighborhood of A, the load F_1 is tensile ($F_1 > 0$) for $b_1 > b_1^0$, and compressive ($F_1 < 0$) for $b_1 < b_1^0$. In Figs. 2 and 3, the curves of force and energy versus b_1 give the impression of being very "flat or shallow" in the vicinity of A; however, this impression is somewhat misleading because the ordinate scales for these quantities cover a very large range of values. [Other curves, to be discussed shortly (viz., Figs. 5 and 9) show these quantities in a somewhat different perspective.]

Throughout the range of deformation between states P and B, in Figs. 2 and 3, the criteria (9) are satisfied and, accordingly, the Hessians

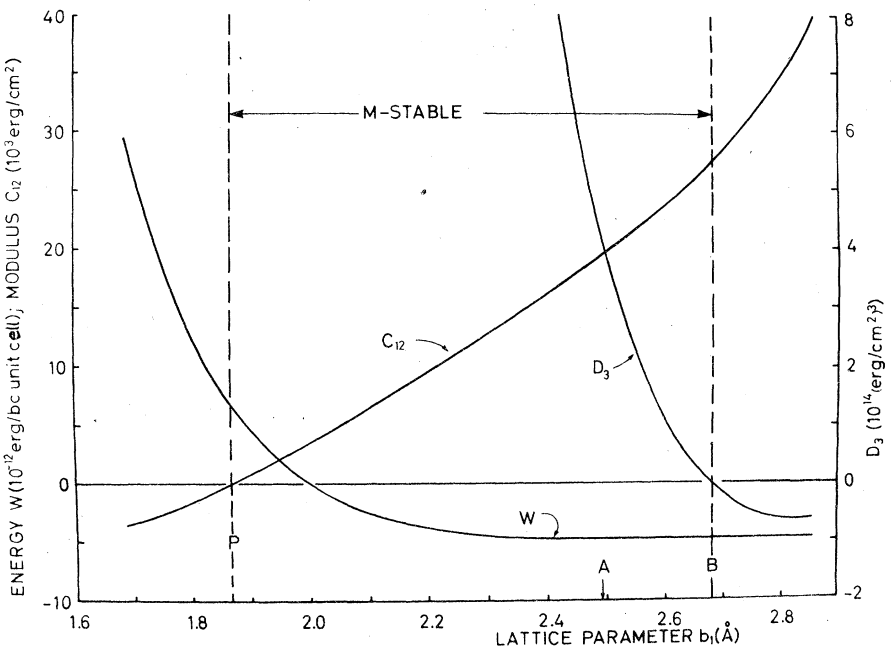

FIG. 2. Internal energy per unit bc cell, modulus C_{12}, and 3×3 determinant D_3 vs lattice parameter b_1.

$C_{rs}\,\delta q_r\,\delta q_s$ are positive definite. The Hessians become semidefinite at states P and B, where the conditions $C_{12}>0$ and $D_3>0$ are violated, respectively. From (8), the former condition is equivalent to $C_{66}>0$. In compression, at state P, the critical variation δq_r that causes the semidefinite Hessian $C_{rs}\,\delta q_r\,\delta q_s$ to vanish is $\delta q_r=0$ for $r\neq 6$ and $\delta q_6\neq 0$, where q_6 is the angle between edges b_1 and b_2. This eigensolution represents a shear, parallel to the reference axes of the bc cell in the 1-2 plane.

In tension, state B occurs at the point of maximum force F_1 in Fig. 3; at that point, the critical variation δq_r that causes the Hessian to vanish is the actual variation along the primary path, viz.,

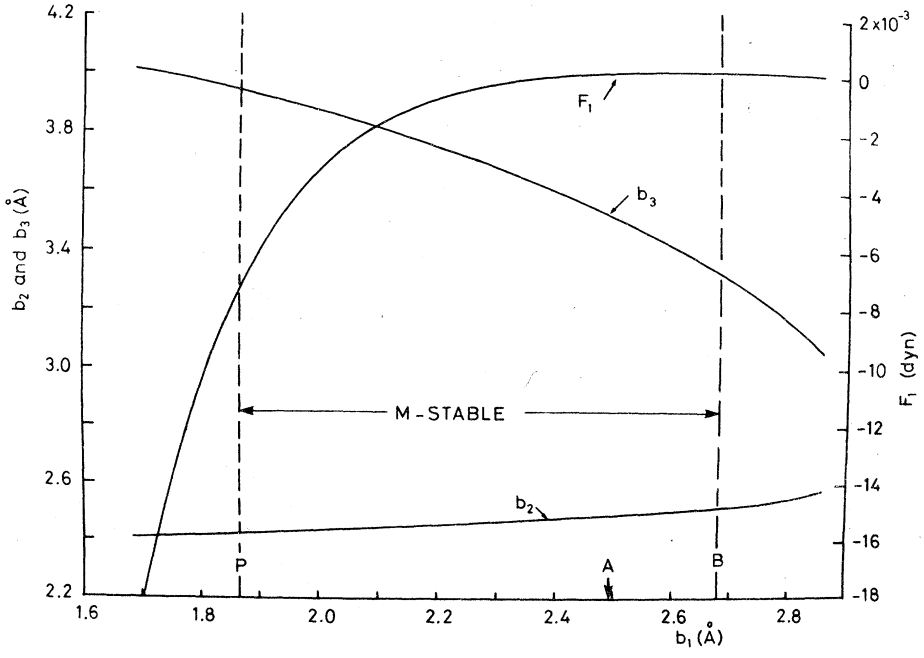

FIG. 3. Applied force F_1 acting on the face of a bc cell and lattice parameters b_2 and b_3 vs b_1.

$$\begin{aligned}
\delta q_1 &= \delta b_1 , \\
\delta q_2 &= [(C_{13}C_{23} - C_{12}C_{33})/(C_{22}C_{33} - C_{23}^2)]\,\delta b_1 , \\
\delta q_3 &= [(C_{12}C_{23} - C_{13}C_{22})/(C_{22}C_{33} - C_{23}^2)]\,\delta b_1 , \\
\delta q_4 &= \delta q_5 = \delta q_6 = 0 .
\end{aligned} \tag{10}$$

The maximum force F_1 at this point is $=7.36\times10^{-5}$ dyn, the corresponding stress $\sigma_{110}=8.78\times10^{10}$ dyn/cm^2, and the stretch $b_1/b_1^0=1.0752$. These values compare reasonably well with various estimates of the theoretical strength of crystals, including the strengths of whiskers, which have exhibited maximum stresses in the range of about 1.7×10^{10} dyn/cm^2 (for Ag) to about 13.1×10^{10} dyn/cm^2 (for Fe), with corresponding strains estimated to be at least (3–5)%.[9-11] These values are also comparable to (although somewhat less than) the values calculated for the same crystal model, loaded uniaxially in the [100] direction (i.e., parallel to a cube edge in the fc cell), at the limit of M stability in tension, viz., $\sigma_{100}=16.78\times10^{10}$ dyn/cm^2 at a stretch $a_1/a^0=1.107$, where a_1 is the edge of the fc cell parallel to σ_{100}.

One aspect of Figs. 2 and 3 that is particularly noteworthy is the very large values of compressive load and strain that occur at the limit of M stability in compression; at state P, $F_1=-7.34\times10^{-3}$ dyn, $\sigma_{110}=-7.68\times10^{12}$ dyn/cm^2, and the stretch $b_1/b_1^0=0.7490$. The magnitude of this compressive stress is about one hundred times greater than the stress at the limit of M stability in tension (which, as has been noted, is comparable to various estimates of the theoretical ultimate strength of crystals). Intuitively, one might expect very much larger values of theoretical crystal strength in compression, at least for some modes of loading. Nevertheless, the present calculations are apparently the first to have given any indication of theoretical "stability" at such very large compressive stresses.

Previous studies,[2,6] involving uniaxial compression, had the applied load parallel to a cube edge of an fcc lattice. In those studies, the *compressive* stresses that were obtained at the limit of M stability[2,5] (occurring at a force minimum) and at the limit of G stability[5,6] (occurring at a minimum of the Green's conjugate stress) were comparable in magnitude to the maximum stresses in *tension* along the primary path as well as to the stresses at the limits of M stability or G stability in *tension* (the latter stresses were somewhat less than the maximum tensile stresses). However, as was shown by Milstein's studies[1,2] of [100] loading of a bcc and fcc crystal, the range of stability of the fcc lattice in this mode of compression is limited by the appearance of a transition to the stress-free bcc state along the primary path of deformation, and the stress and force minima mentioned above are a natural consequence of this transition.

In the present calculations, no such stress-free states or force minima appeared in the compression region (starting from state A); calculations were made in this region for values of b_1 as small as 0.75 Å. Even at the smallest values of b_1, the quantities $-F_1$, $-\sigma_{110}$, D_2, D_3, and all of the elastic moduli C_{ij} (with the exceptions of C_{12} and C_{13}) are positive and increasing with further compression. Although C_{13} remains positive throughout this compressive range, its magnitude appears to approach zero asymptotically with decreasing b_1. The only criterion for M stability that is violated in the compressive range (along this path) is $C_{12}\leq 0$ at, and to the left of, state P. The quantity C_{12} reaches a minimum at $b_1=1.49$ Å, and with further compression also appears to approach zero asymptotically (although from the negative).

Another interesting feature of the [110] loading of the crystal, shown in Fig. 3, is the difference in the algebraic signs of the Poisson's ratio ν along the b_2 and b_3 axes. The principal stretches, normal to the applied loads, at the limits of M stability are $b_2/b_2^0=1.0106$ and $b_3/b_3^0=0.9446$ in tension (at B), and $b_2/b_2^0=0.9734$ and $b_3/b_3^0=1.1180$ in compression (at P). Increasing tension, say, in the vicinity of state A, results in a decrease of b_3 and an increase of b_2. Such behavior is apparently characteristic of an actual (i.e., a real) Ni crystal (as well as of the present model), as can be seen from substituting experimental values of elastic constants into the linear elasticity expressions for the initial values of the directional Poisson's ratios. That is, along the b_2 axis,

$$\nu = -\frac{\delta b_2/b_2^0}{\delta b_1/b_1^0} = \frac{R-2C_{44}}{R+2C_{44}} = -0.051 ,$$

and, along the b_3 axis,

$$\nu = -\frac{\delta b_3/b_3^0}{\delta b_1/b_1^0} = \frac{4C_{12}C_{44}}{C_{11}(R+2C_{44})} = 0.607 ,$$

where $R=C_{11}+C_{12}(1-2C_{12}/C_{11})$ and (here only) the C_{ij} represent experimental values[12] of the usual elastic moduli (i.e., the zero-load Green's moduli at 0 °K) relative to the fcc unit cell, viz., $C_{11}=2.612$, $C_{12}=1.508$, and $C_{44}=1.317$, in units of 10^{12} dyn/cm^2. Also (here only), the δb_i are the initial variations along the primary path, starting from state A.[13,14]

For curiosity we also calculated, in the above manner, the initial Poisson's ratios for a number of other fcc metals. In all cases ν was found to be positive along the b_3 axis, while along b_2, ν was positive for Al, Au, and Pd, and negative for Cu, Pb, and Ag (as well as Ni); in each case, the magnitude of ν along b_2 was less than that along b_3.

It might be of interest to mention some additional observations about the behavior of the lattice, particularly at very large compressive strains, along the primary equilibrium (but not necessarily stable) path that is reached by starting from state A and repeatedly decreasing b_1 while adjusting b_2 and b_3 to insure uniaxial force $F_1 \neq 0$, in general, while $F_2 = F_3 = 0$, always. First, as b_1 decreases, b_2 continues to decrease and b_3 to increase (at a faster rate than b_2 decreases) throughout the range of compression investigated (to about $b_1 = 0.75$ Å). Second, the Poisson's ratio appears to approach zero asymptotically along both principal axes normal to the load (i.e., b_2 and b_3 appear to approach constant values) at very high compressive strains. This observation is consistent with the earlier mentioned observation that C_{12} and C_{13} appear to approach zero asymptotically as b_1 becomes small. That is, if δF_i represents a small variation in force F_i at some point along the equilibrium path, and δb_i are the corresponding small variations in the b_i, then to first order in the δ quantities, $\delta F_i = C_{ij}\delta b_j$. Thus, if $C_{12} = C_{13} = 0$, along the primary path, (i) $\delta F_1 = C_{11}\delta b_1$ (independent of δb_2 and δb_3); (ii) $\delta F_2 \equiv 0 = C_{22}\delta b_2 + C_{23}\delta b_3$; and (iii) $\delta F_3 \equiv 0 = C_{23}\delta b_2 + C_{33}\delta b_3$. Conditions (ii) and (iii) are, of course, satisfied by $\delta b_2 = \delta b_3 = 0$. Thus, b_2 and b_3 remain constant along the primary path if $C_{12} = C_{13} = 0$. Third, as b_1 decreases, the ratio of b_3 to b_2 seems to be approaching $\sqrt{3}$; e.g., at b_1 equal to about 1 Å, $(b_3/b_2)^2 = 2.997$, and at b_1 equal to about 0.75 Å, $(b_3/b_2)^2 = 2.99996$. Thus, throughout the compressive region, the ratio b_3/b_2 apparently remains between $\sqrt{2}$ (the initial value at A) and $\sqrt{3}$. Although this behavior (i.e., b_3/b_2 approaching $\sqrt{3}$) was first noticed empirically, it can be readily understood as the tendency of the atoms in successive planes, normal to the load, to form a close-packed pattern as the planes approach one another. That is, the two-dimensional lattice, formed by projecting the lattice sites of the three-dimensional lattice onto a plane perpendicular to the load, becomes close packed (i.e., each lattice site in this two-dimensional lattice has six equidistant nearest-neighbor sites) at large compressive strains. Thus, in a sense, the difference in the signs of the Poisson's ratios in the b_2 and b_3 directions (at least in the region of high compression) can be understood as the tendency of the atoms in successive planes to arrange themselves in such a close-packed relationship as the compressive load increases in magnitude.

Examination of Fig. 3 leads us to presume that, generally, for a fcc lattice loaded uniaxially in a [110] direction, the values of b_2 and b_3 will eventually become equal at some point along the equilibrium (although not necessarily stable) path of deformation. (In principle, a possible exception might be a crystal for which the b_2 curve remains parallel to the b_3 curve, or the two curves diverge, as b_1 increases *and* decreases.) In view of the probable generality of this occurrence (i.e., b_2 and b_3 becoming equal) and (with the benefit of hindsight) in view of the special nature of the bifurcation that was found at the point at which b_2 and b_3 first become equal, we now examine, in detail, this occurrence and its effect upon the primary equilibrium paths.

From general considerations, once the state at which $b_2 = b_3$ is reached, it follows that there must be a branch of the primary equilibrium path, along which b_2 remains equal to b_3, which can be reached from state A by moving along the path for which $b_2 \neq b_3$. In other words, there must be at least two branches of the primary equilibrium path (defined by the conditions $F_2 = F_3 = 0$ and b_1, b_2, and b_3 mutually perpendicular) that intersect at the point at which $b_2 = b_3$ on both branches; along one branch, $b_2 \neq b_3$, in general, and along the other, $b_2 = b_3$. Furthermore, the latter branch (i.e., $b_2 = b_3$) is the same as the primary path that would be obtained for [100] *loading* of a fcc crystal, prescribed by the following conditions. If a_1, a_2, and a_3 represent the edges of the fc cell, then in the unloaded fcc state $a_1 = a_2 = a_3$; along the path in general the load is applied parallel to the edge a_1; the forces or stresses parallel to the edges a_2 and a_3 are zero; $a_2 = a_3$; and the edges a_1, a_2, and a_3 are mutually perpendicular. For the present crystal model, this [100] loading path was studied in detail in Ref. 2. This equivalence between the [100] and [110] loading of a fc lattice along the branch $b_2 = b_3$ is illustrated in Fig. 4, which shows four of the bc cells and also shows the orientation of a fc cell with respect to the bc cells. Along the branch $b_2 = b_3$, the symmetries of both the bc and the fc cells are at least tetragonal.

Figure 5 shows the energy W per unit bc cell and the applied load F_1 acting on the face of the cell along both branches of the primary path. Along branch $ABCD$, $b_2 \neq b_3$ (except at state D where the two branches meet) and along branch $FGHDIJ$, $b_2 = b_3$. (The W and F_1 ordinate scales in Fig. 5 are markedly different from those in Figs. 2 and 3 since the latter were selected with the intention of displaying phenomena near the limit of M stability in compression at P, where there were very large compressive forces.) A number of stress-free states are observed, viz., A, C, G, I, and J. The stress-free states along the "$b_2 = b_3$" branch have been identified previously[2] as the fcc state (G), the bcc state (I), and a

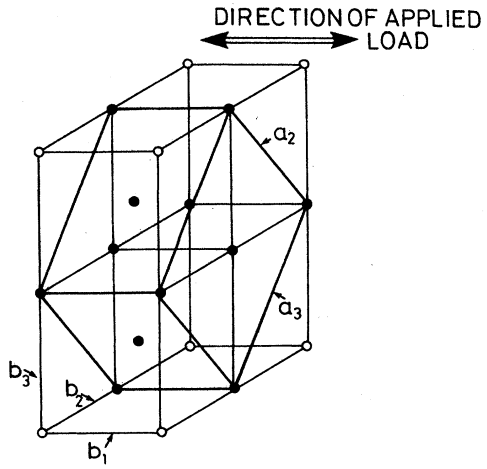

FIG. 4. Illustration of the fc cell ("solid centers") that becomes tetragonal (edges mutually perpendicular and $a_2 = a_3$) when $b_2 = b_3$.

tetragonal state without any apparent higher symmetry (J). The orientation of the fcc cell in state G, with respect to the edges b_i of the bc cell, is indicated by the orientation of the fc cell in Fig. 4. Except for a spatial rotation, the fcc states G and A are identical. In the stress-free bc state I, the cube edge $b_1 = b_2 = b_3 = 2.8138$ Å,[15] and in state J, $b_1 = 2.6247$ Å, $b_2 = b_3 = 2.9143$ Å. Along the "$b_2 \neq b_3$" path, state A has already been identified as the "starting fcc state," with the fcc cell orientated as in Fig. 1; the other zero stress state is C, where $b_1 = b_3 = 2.9143$ Å, $b_2 = 2.6247$ Å. Thus, except for a rotation in space, states C and J are identical. The zero-stress tetragonal configuration appears at a local energy minimum (state J) along the "$b_2 = b_3$" path and at a local energy maximum (state C) along the "$b_2 \neq b_3$" path. The bcc state (I) also occurs at a local energy maximum along the primary path.

The limits of M stability along the "$b_2 = b_3$" branch are at H (in compression, $F_1 < 0$) and F (in tension, $F_1 > 0$). In Ref. 2, these states were identified as the states at which $C_{11}(C_{22} + C_{23}) - 2C_{12}^2 = 0$ (state H) and $C_{22} - C_{23} = 0$ (state F), where the C_{ij} of Ref. 2 are the M moduli relative to the fc cell. State H occurs at a local force minimum,[16] and at this state, the particular eigensolution causing the semidefinite $C_{rs}\delta q_r \delta q_s$ to vanish is[5] $\delta q_r \propto (2C_{12}, -C_{11}, -C_{11}, 0, 0, 0)$, i.e., the critical variation is the same as the actual variation along the primary path.[5] The critical variation at state F, relative to the M variables and the fc cell, was identified in Ref. 2 as $\delta a_2 = -\delta a_3$, i.e., $\delta q_r \propto (0, 1, -1, 0, 0, 0)$. In Ref. 5, it was shown that this type of eigenstate (i.e., $C_{22} = C_{23}$), together with the eigensolution, is invariant (i.e., its location, on the primary path of [100] loading of a cubic crystal, will be the same for any reasonable choice of strain variables). In the present study, state F appears at $C_{23} = 0$, which is the same as $C_{44} = 0$ [from (8)], relative to the bc unit cell, with the corresponding eigensolution $\delta q_r \propto (0, 0, 0, 1, 0, 0)$, where δq_4 is the angle between b_2 and b_3. The eigensolution represents a shear parallel to the reference axes in the 2-3 plane, which, to first order in the δ quantities, is the same as the variation $\delta q_r \propto (0, 1, -1, 0, 0, 0)$ relative to the fc cell. The proof of the invariance of the $C_{22} = C_{23}$ eigenstate in Ref. 5 assumes a cubic cell as a reference basis with "coordinates assigned so that q_4, q_5, q_6 remain fixed and equal when the cell stays rectangular, while generally each of the groups q_1, q_2, q_3 and q_4, q_5, q_6 accord equal weightings to the

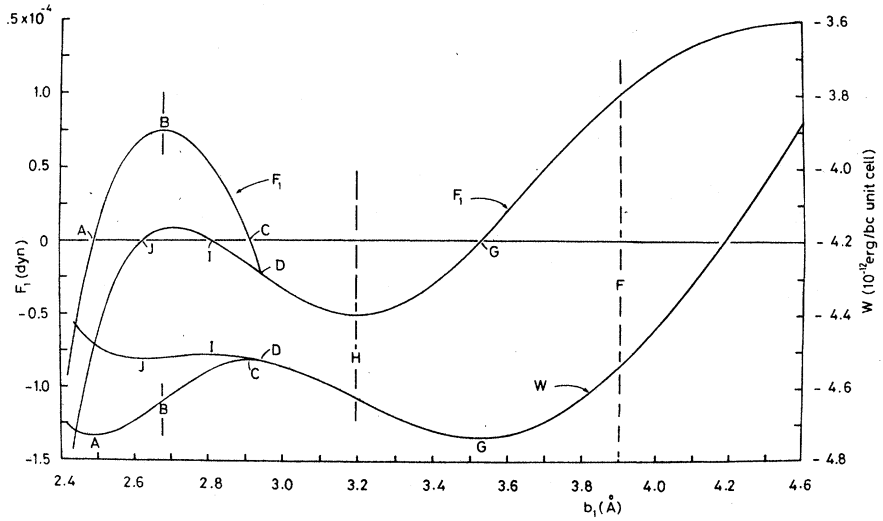

FIG. 5. Energy per unit bc cell and applied force acting on the face of the cell along two branches of the primary equilibrium path. Along branch . . .$FGHDIJ$. . ., $b_2 = b_3$; along branch . . .$ABCD$, $b_2 \neq b_3$ (except at D).

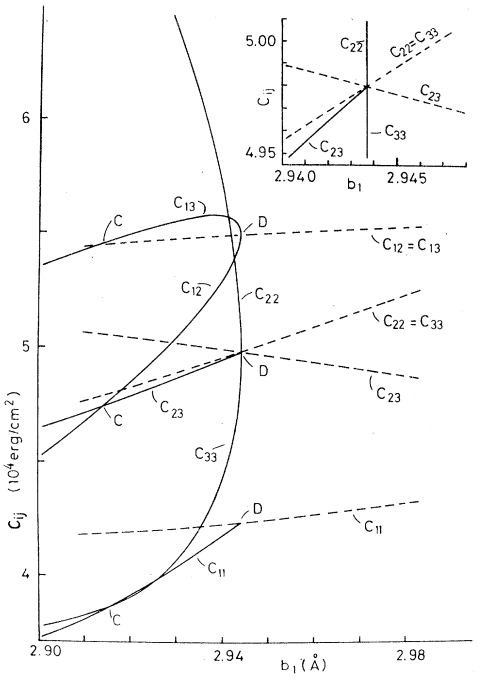

FIG. 6. Elastic moduli in the neighborhood of the intersection (at D) of the two branches of the primary equilibrium path. The moduli along the "$b_2=b_3$" branch are indicated by "broken line" curves and those along the "$b_2\neq b_3$" branch by "solid line" curves. From symmetry at state D ($b_2=b_3$), it follows that $C_{12}=C_{13}$ and $C_{22}=C_{33}$; in addition, the theoretical calculations show that state D coincides with the invariant eigenstate $C_{22}=C_{23}$. State C ($b_1=b_3$ and hence $C_{11}=C_{33}$; $C_{12}=C_{23}$) is also indicated on the "$b_2\neq b_3$" branch.

three cubic directions." For the [110] loading of a fcc crystal, one may select the bcc state (as at I, in Fig. 5) or the fcc state (as at G) as the reference state, and accordingly, define the edges of either the bcc or the fcc cell as the three cubic reference directions. Thus, along the primary [100] loading path (of, say, force or stress versus lattice parameter), the "invariant" $C_{22}=C_{23}$ eigenstate, relative to, say, the bc cell, will appear at the same point on the path as the $C_{44}=0$ eigenstate relative to the fc cell, and vice versa.

We now focus our attention on the behavior in the immediate neighborhood of state D. Figure 6 shows the M moduli (relative to the bc cell) versus b_1, along both branches near state D. The path branching at D is found to be a bifurcation associated with the invariant eigenstate $C_{22}=C_{23}$ (relative to the bc cell). That is, at state D, $C_{22}=C_{23}$, and the bifurcation leading from path $\ldots HDI\ldots$ to path $DCB\ldots$ is of the type $\delta b_2=-\delta b_3$; $\delta b_1=0$ (b_2 and b_3 approach one another with infinite slopes, with respect to b_1, as state D is approached along $\ldots BCD$). For such bifurcation, viewed as leading from the "$b_2=b_3$" path to the "$b_2\neq b_3$" path, it is immaterial whether one considers that δb_3 is negative, say, and δb_2 positive, or vice versa. (Indeed, the choice of which of the two lattice parameters, perpendicular to the load, is to be called b_2 and which b_3 is entirely immaterial along path $\ldots HDI\ldots$.) From this consideration, it follows that the path $\ldots ABCD$ represents only one half of the full branch $\ldots ABCDC'B'A'\ldots$, such that, if the lattice moves along the path in the direction $DC'B'\ldots$, then b_3 decreases and b_2 increases, while in the direction $DCB\ldots$, the reverse is true. In other words, the lattice parameter b_2 can be thought of as continually increasing and b_3 continually decreasing along the path $\ldots BCDC'B'\ldots$. It also follows that the portion of the branch $DCBA\ldots$ bears a special relationship to the portion $DC'B'A'\ldots$, viz., if a state Q, with lattice parameters $(b_1, b_2, b_3)=(\beta_1, \beta_2, \beta_3)$, is an equilibrium state along path $DCBA\ldots$, then Q', with lattice parameters $(\beta_1, \beta_3, \beta_2)$, is a corresponding equilibrium state on the portion $DC'B'A'\ldots$. Figure 7 shows this relationship among the lattice parameters along the full branch $PABCDC'B'A'P'$. In this figure, the three-dimensional space curves (b_1, b_2, b_3) for both branches (i.e., $\ldots DIJ\ldots$ and $\ldots CDC'\ldots$) are projected onto the "faces of a box," the edges of which form the Cartesian coordinate system b_1, b_2, b_3, and

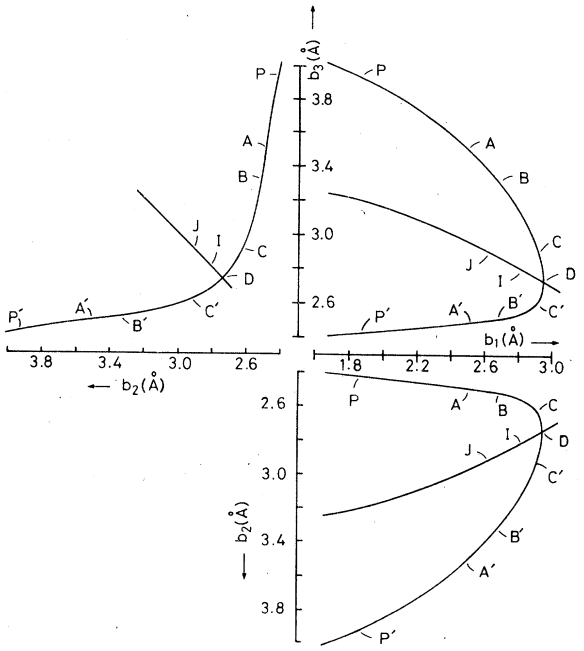

FIG. 7. Variation of the lattice parameters b_1, b_2, and b_3 of the bc cell along the primary equilibrium path.

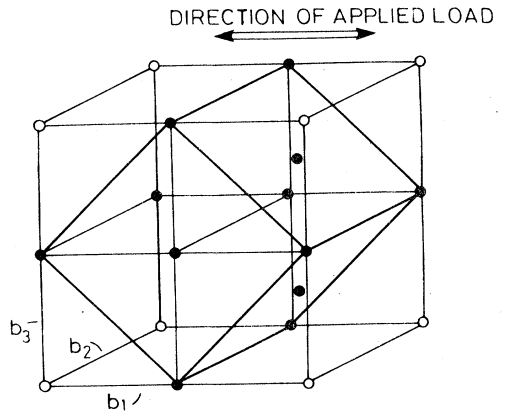

FIG. 8. Illustration of the fc cell ("solid centers") that becomes cubic in state A'.

the faces of the box are "unfolded" for a two-dimensional representation of the simultaneous variation of the three variables. States A' and C' are the stress-free fcc and tetragonal states, respectively. Starting at state A, where the fcc unit cell has the orientation as shown in Fig. 1, and moving along the primary path $ABCDC'B'A'$ to the state A', results in the fcc cell at A' orientated as shown in Fig. 8. The crystal is M stable in the ranges between states P' and B' (as well as between P and B). Because of the "interchange" of the roles of b_2 and b_3 along the regions $DCBA\ldots$ and $DC'B'A'\ldots$, the elastic moduli C_{ij} in state Q are related to the elastic moduli C'_{ij} in state Q' (where the numerical value of b_1 is the same as at Q, but the values of b_2 and b_3 are interchanged) by the relations

$$\begin{aligned} &C'_{11}=C_{11},\quad C'_{23}=C_{23},\quad C'_{13}=C_{12},\\ &C'_{12}=C_{13},\quad C'_{33}=C_{22},\quad C'_{22}=C_{33}. \end{aligned} \tag{11}$$

It is noted in Fig. 6 that C_{22} and C_{33} approach one another with infinite slope at state D along path $\ldots BCD$, likewise for C_{13} and C_{12}. This behavior is consistent with the last four relationships in (11).

The applied force and internal energy, when plotted versus b_1, will appear identical along $\ldots ABCD$ and $\ldots A'B'C'D$. Thus states A and A', etc., coincide in Fig. 5. However, this "degeneracy" is removed when the force or energy is plotted versus b_2 or b_3. For example, Fig. 9 shows the applied force versus b_2. (The identical curve would appear for the applied force versus b_3; however, A and A' would exchange places, as would B and B', etc.) At state D, along path CDC', the force is, of course, stationary, i.e., $\delta F_i = C_{ij}\delta b_j = 0$ along the primary path at that point (since $C_{13}=C_{12}$; $C_{33}=C_{22}=C_{23}$; $\delta b_1 = 0$; $\delta b_2 = -\delta b_3$). The reason that the force does not "give the appearance" of being stationary on path $DC\ldots$ at state D in Fig. 5 is simply because the first-order variation in the b_i along the primary path at that point has $\delta b_1 = 0$. Also, in Fig. 5, it is interesting to note that the energy curves approach one another with the same slope at D (along both branches), although the force curves have different slopes at D. At any stage on the primary path $\ldots ABC\ldots$, $\delta F_1 = C_{1r}\delta q_r$, where the δq_r are given by (10); an incremental change in energy, complete to second-order terms is[5] $\delta W = F_1\delta b_1 + \frac{1}{2}\delta F_1 \delta b_1$. Thus, along the path $\ldots ABC\ldots$,

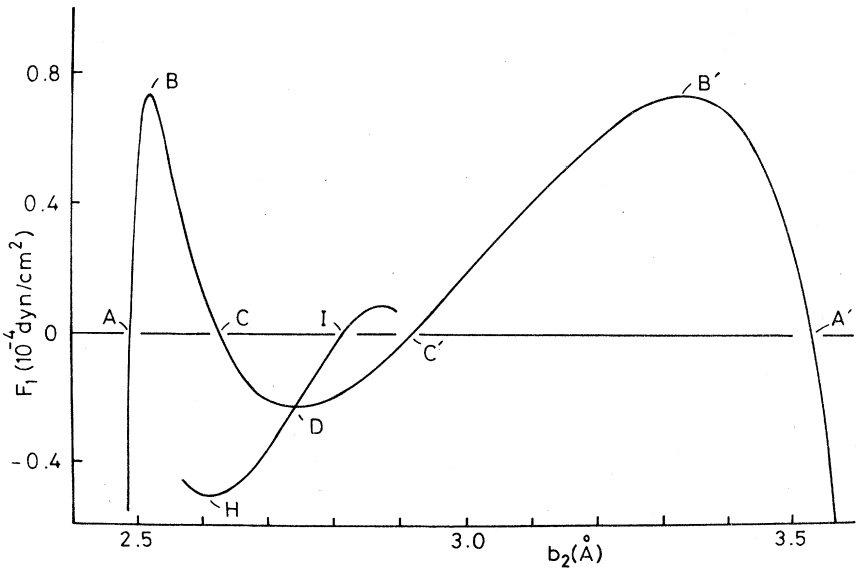

FIG. 9. Applied force vs lattice parameter b_2.

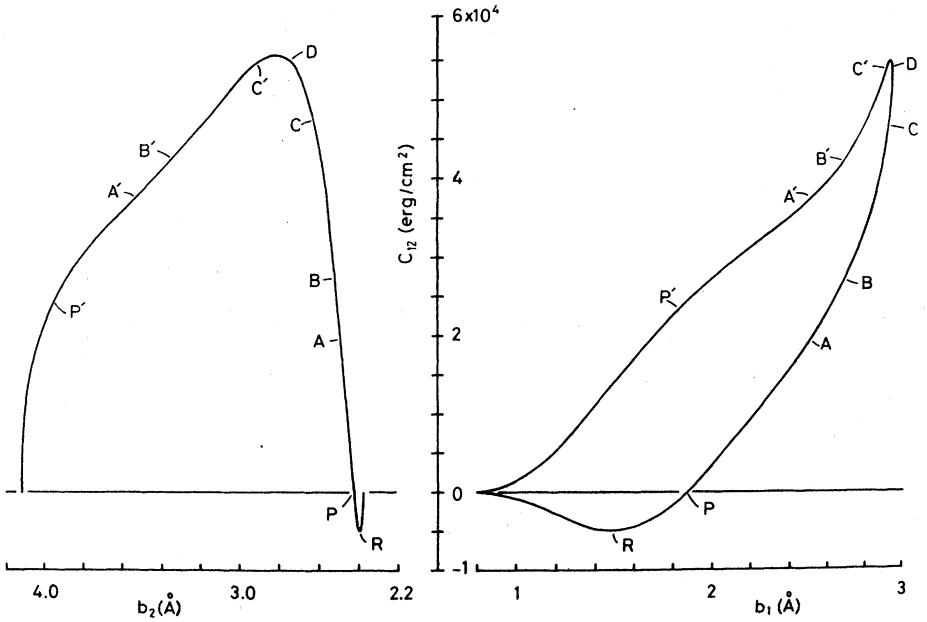

FIG. 10. Modulus C_{12} vs b_1 and b_2. The plot of C_{12} vs b_1 is identical to C_{13} vs b_1 (with states P and P', etc., interchanged).

$$\delta W = F_1 \delta b_1 + \tfrac{1}{2}\{C_{11} + [(C_{13}C_{23} - C_{12}C_{33})/(C_{22}C_{33} - C_{23}^2)]C_{12} + [(C_{12}C_{23} - C_{13}C_{22})/(C_{22}C_{23} - C_{23}^2)]C_{13}\}\delta b_1^2 . \quad (12)$$

The same relation also holds along the path $\ldots FGH\ldots$, although with the added symmetry $C_{22} = C_{33}$ and $C_{12} = C_{13}$; thus along $\ldots FGH\ldots$

$$\delta W = F_1 \delta b_1 + \tfrac{1}{2}\{C_{11} - 2C_{12}^2/(C_{22} + C_{23})\}\,\delta b_1^2 . \quad (13)$$

The slope of the W-vs-b_1 curve, for both branches, is thus simply F_1. The slope of W vs b_2 (or b_3), however, is not the same for both branches at D; this is easily seen from the fact that the magnitude of δb_2 (or δb_3) at state D is much larger along path $\ldots CDC'\ldots$ than along $\ldots HDI\ldots$ for a given small δb_1. The quantity within the brackets $\{\ \}$ in (12) or (13) is $\delta F_1/\delta b_1$ along the respective branches; thus, in general, this quantity represents the slope of the F_1-vs-b_1 curve at any stage. However, at state D, along path $\ldots CDC'\ldots$, both F_1 and b_1 are stationary, and the quantity within the $\{\ \}$ in Eq. (12) is not determinate from the values of the first-order C_{ij} at state D (although this quantity can, of course, be determined directly from our F_1-vs-b_1 calculations near D).

Although (in the present study) state D is em-

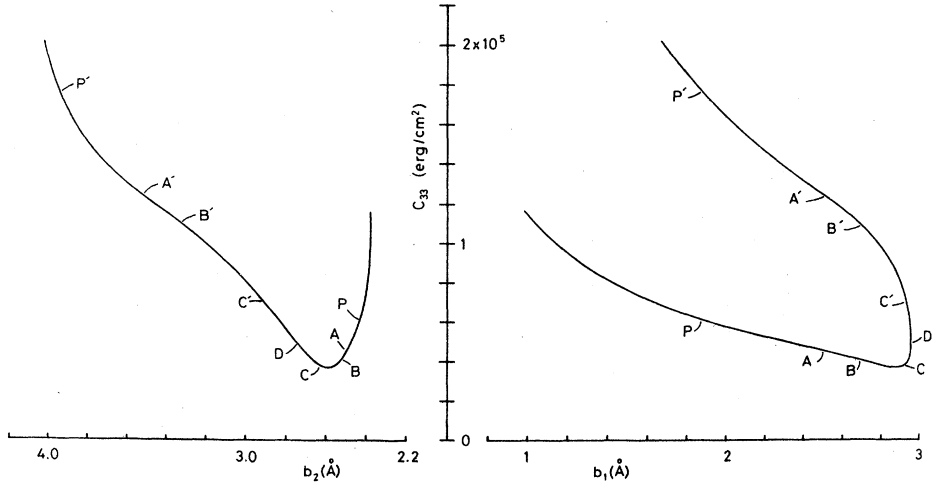

FIG. 11. Modulus C_{33} vs b_1 and b_2. The plot of C_{33} vs b_1 is identical to C_{22} vs b_1 (with states P and P', etc., interchanged).

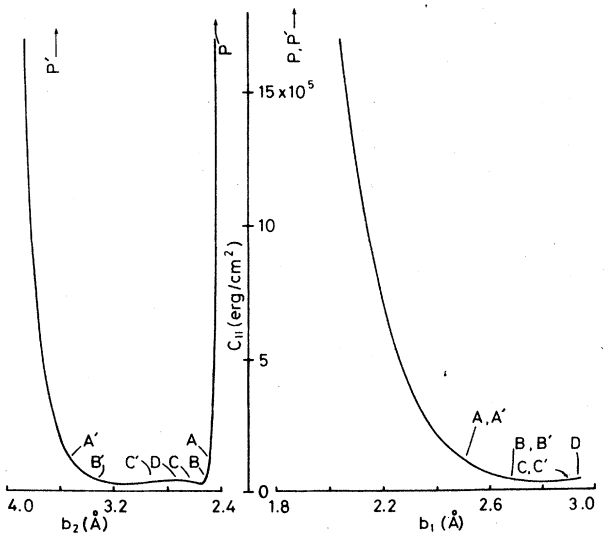

FIG. 12. Modulus C_{11} vs b_1 and b_2.

bedded in an unstable region, for some other crystal (with, e.g., different values of the initial elastic moduli and directional Poisson's ratios), such a state could terminate a stable region along one of the branches of the primary path; thus, we have described the phenomena occurring in the neighborhood of state D in considerable detail. As an example, in the [100] loading calculations of Ref. 1 (where the bcc state itself was in a stable region), the eigenstate $C_{22}=C_{23}$ (relative to the bc cell) terminated a stable range in compression. For that particular crystal model, it is quite likely that this state is also at the intersection of the two branches of the [110] loading path, as in the present case.

Finally, Figs. 10–15 display the moduli C_{ij}, D_2, and D_3 along the primary path $\ldots ABCDC'B'A'\ldots$. The figures are of the "folding-box type," which show the behavior versus b_1 and b_2. Plots of C_{22} and C_{13} are not included, since a plot of C_{22} vs b_1 is identical to a plot of C_{33} vs b_1 with P and P', A and A', etc., interchanged, likewise for C_{12} and C_{13}. This "identicalness" of the C_{12}- and C_{13}-vs-b_1 plots and C_{22}- and C_{33}-vs-b_1 plots follows directly from the last four relations in (11). Also, the plots of C_{12} and C_{33} vs b_2 are the same as plots of C_{13} and C_{22}, respectively, vs b_3, with P and P', A and A', etc., interchanged.

The curves of Figs. 10–15 can be classified according to two types of symmetries; the first type is for quantities which become different quantities when the subscripts 2 and 3 are interchanged (viz., C_{12}, C_{33}, and D_2), and the second is for quantities which are invariant with respect to interchange of the indices 2 and 3 (viz., C_{11}, C_{23}, and D_3). (Interchanging indices 2 and 3 in the three by three determinant D_3 is equivalent to interchanging the last two rows and then the last two columns of the determinant, which, of course, leaves it unchanged.) Plots of quantities with the second type of symmetry (Figs. 12–14) have the following characteristics. States P and P', A and A', etc., are at the same point on the plot versus

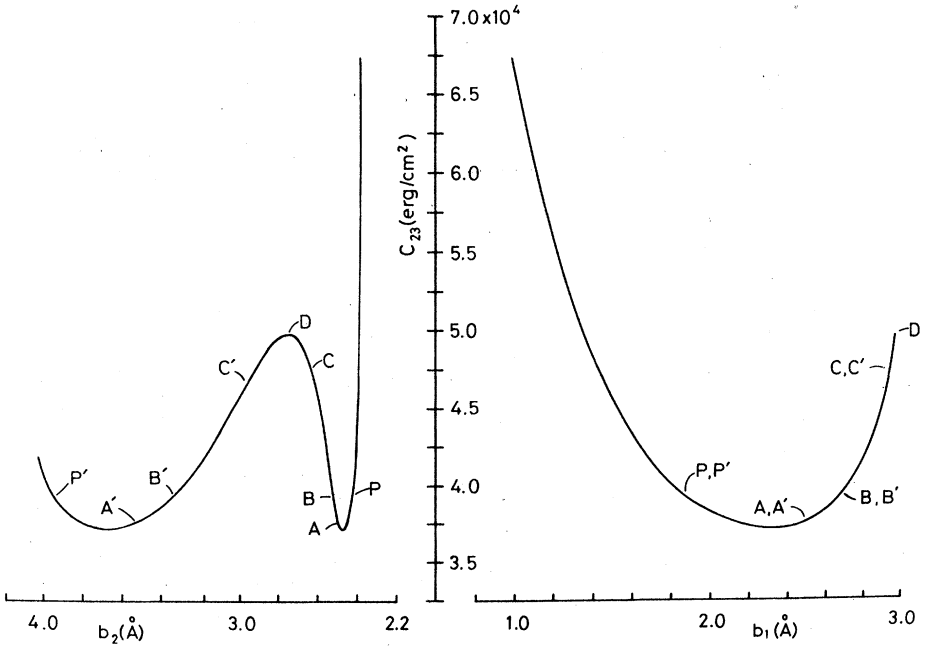

FIG. 13. Modulus C_{23} vs b_1 and b_2.

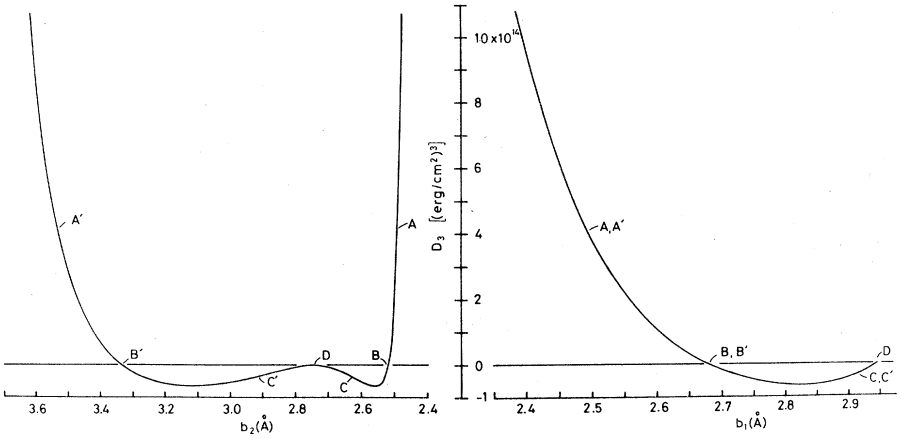

FIG. 14. 3×3 determinant D_3 vs b_1 and b_2.

b_1; the plot versus b_1 "appears" to end abruptly at state D while the plot versus b_2 is stationary at D (since the variation at state D along the equilibrium path is $\delta b_1 = 0$, $\delta b_2 = -\delta b_3$, the quantities are stationary at D along the path). In plots of the remaining quantities (Figs. 10, 11, and 15), states P and P', etc., appear at the same value of b_1 (by definition), but not at the same points in the plots versus b_1; the slopes of these curves are infinite at state D in the plots versus b_1; the quantities are not stationary at D. The plot of D_2 vs b_1 is identical to a plot of the two by two determinant $C_{11}C_{33} - C_{13}^2$ vs b_1, with states P and P', etc., interchanged.

The determinant D_3 must be zero at state D since $C_{22} - C_{33}$ is one of the factors of this determinant[5] if $C_{22} = C_{33}$ and $C_{12} = C_{13}$ (as at D). Along the path $ABC\ldots$, D_2 passes from positive to negative at $b_1 = 2.931$ Å, reaches a minimum at $b_1 = 2.914$ Å (very close to state C'), and passes from negative to positive at $b_1 = 2.6875$ Å; D_3 is negative throughout the range in which $D_2 \leq 0$ (state B' is at $b_1 = 2.6791$ Å). The behavior of D_2 and D_3 for small values of b_1 is dominated by C_{11}, which increases rapidly as b_1 decreases (the ordinate scale for C_{11}, Fig. 12, is more than an order of magnitude greater than that for any other C_{ij}). C_{11} is positive throughout, with a minimum at $b_1 = 2.82$ Å and a local maximum at D. The other C_{ij} (with the exception of C_{12} and C_{13}) are also positive throughout. C_{12} passes through a maximum at $b_1 = 2.938$ Å, C_{33} a minimum at $b_1 = 2.87$ Å, and C_{23} a minimum at $b_1 = 2.32$ Å. At state D, $b_1 = 2.9437$ Å, and $b_2 = b_3 = 2.742$ Å. The variations of the C_{ij} with

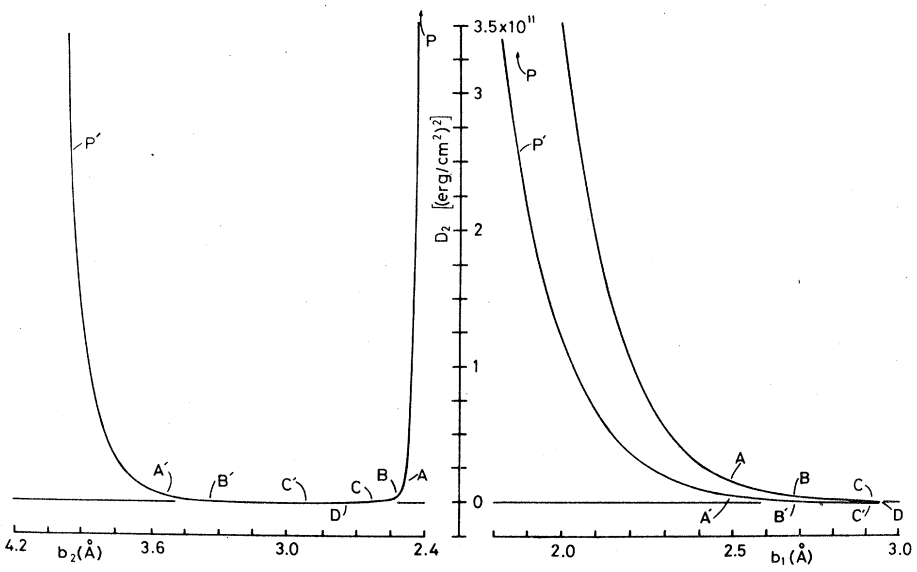

FIG. 15. 2×2 determinant D_2 vs b_1 and b_2.

respect to the b_i are apparently not, in general, readily described (or well approximated) by simple analytical functions throughout the full path $\ldots ABCD\ldots$.

ACKNOWLEDGMENTS

One of us (F.M.) is very grateful for a John Simon Guggenheim Memorial Fellowship and a NATO Senior Fellowship (administered by the NATO Senior Scientists Program), during the tenures of which large portions of this work were completed. Parts of this work were carried out while F. M. was on leave at the Department of Electronics, Weizmann Institute of Science, Rehovot, Israel, and the Department of Applied Mathematics and Theoretical Physics, University of Cambridge, England; gratitude is expressed to these departments, and to one of the Cambridge colleges, Clare Hall, for their support and/or hospitality. We wish to express our deep appreciation to Professor R. Hill, F. R. S., for his active interest in this work and many helpful discussions.

---

*Permanent address

[1]F. Milstein, Phys. Rev. B 3, 1130 (1971).

[2]F. Milstein, J. Appl. Phys. 44, 3833 (1973).

[3]K. Huang, F. Milstein, and J. A. Baldwin, Jr., Phys. Rev. B 10, 3635 (1974).

[4]F. Milstein, J. Appl. Phys. 44, 3825 (1973).

[5]R. Hill and F. Milstein, Phys. Rev. B 15, 3087 (1977).

[6]M. Born and R. Fürth, Proc. Cambridge Philos. Soc. 36, 454 (1940).

[7]N. H. Macmillan and A. Kelly, Proc. R. Soc. A 330, 291 (1972); 330, 309 (1972).

[8]R. Hill, Math. Proc. Cambridge Philos. Soc. 77, 225 (1975).

[9]S. S. Brenner, J. Appl. Phys. 27, 1484 (1956).

[10]S. S. Brenner, Science 128, 569 (1958).

[11]J. C. Crump and J. W. Mitchell, J. Appl. Phys. 41, 717 (1970).

[12]C. Kittel, *Introduction to Solid State Physics*, 4th. ed. (Wiley, New York, 1971).

[13]In the present study, the Poisson's ratio ν is defined as the ratio of the infinitesimal *incremental* strains at any specified stage on the primary loading path, rather than the ratio of the *total* strains. It is clear that the values of ν have opposite algebraic signs along the b_2 and b_3 directions, at any stage on the primary path shown in Fig. 3; likewise, the ratios of the total strains, $(b_2 - b_2^0)/(b_1 - b_1^0)$ and $(b_3 - b_3^0)/(b_1 - b_1^0)$, also have opposite signs at any stage on this path.

[14]Macmillan and Kelly (Ref. 7) studied the behavior of a model NaCl lattice in unconstrained [110] tension, in the range of total [110] strain from zero to about 0.3. Owing to important differences in the nature of the respective crystals, one would not necessarily expect behavior similar to that observed in the present study. Nevertheless, it is interesting to note some similarities and differences. As in the present study, at large strains, their calculations showed ν to be negative along the $[1\bar{1}0]$ axis and positive along the [001] axis (our $[1\bar{1}0]$ and [001] axes, respectively, are b_2 and b_3). However, with increasing [110] strain, the magnitude of ν along their $[1\bar{1}0]$ axis seems to be decreasing slightly, whereas it increases rapidly in the present study. Their initial magnitude of ν along the [001] axis was considerably larger than that along the $[1\bar{1}0]$ axis (as in the present study), although initially their lattice exhibited a positive value of ν in the $[1\bar{1}0]$ direction (in contrast with the present case). Macmillan and Kelly (Ref. 7) also studied [110] loading of a model argon lattice, although not unconstrained (as in their NaCl calculations and as in the present study).

[15]In Ref.2, the bcc cube edge was reported as 2.8134 Å instead of 2.8138 Å; this small difference resulted from different numerical iterative techniques for "zeroing in" on the stress-free lattice parameters; in the previous study, a (slightly less accurate) graphical interpolation was used; in the present study the numberical interpolation was done entirely on the computer.

[16]In the discussion of Ref. 2, there is some ambiguity over whether the state identified as H in the present study occurs at a minimum of the load or of the stress. This was clarified in Ref. 5. For [100] uniaxial loading of a cubic crystal, the condition $C_{22} + C_{23} = 2C_{12}^2/C_{11}$ occurs when the applied load is stationary if the C_{ij} are the M moduli, and when the Green's conjugate stress is stationary, if the C_{ij} are the Green's moduli.